PHYSICAL REVIEW B **75**, 121304(R) (2007)

Room temperature ferromagnetism in Co-doped CeO_2 films on Si(001)

V. Fernandes, J. J. Klein, N. Mattoso, and D. H. Mosca*
Laboratório de Nanoestruturas para Sensores, PIPE-UFPR, 81531-990 Curitiba, Paraná, Brazil

E. Silveira, E. Ribeiro, and W. H. Schreiner
Departamento de Física, Universidade Federal do Paraná, 81531-990 Curitiba, Paraná, Brazil

J. Varalda and A. J. A. de Oliveira
Departamento de Física, Universidade Federal de São Carlos, 13565-905, São Carlos, São Paulo, Brazil
(Received 1 December 2006; revised manuscript received 15 February 2007; published 23 March 2007)

We investigate the room temperature ferromagnetism of nanocrystalline Co-doped CeO_2 films electrodeposited onto Si(001) substrates. The nanocrystalline CeO_2 films, containing from 0.5 to 13.2 at. % Co, present oxygen-vacancy formation with a considerable inclusion of Co into the lattice without evidence of metallic Co clusters or secondary phase formation. We correlate the robust ferromagnetism of this multifunctional magnetic oxide integrated on Si with two exchange mechanisms mediated by intrinsic defect centers observed in the emerging ferromagnetic insulators.

DOI: 10.1103/PhysRevB.75.121304 PACS number(s): 75.50.Dd, 75.30.Hx, 81.15.Pq

Ferromagnetism in diluted magnetic oxides has attracted considerable interest due to the potential application for spintronics with room temperature functionality.[1] There have been several reports on thin films of wide-band-gap semiconductor oxides doped with a few atomic percent of transition metals exhibiting ferromagnetism with a Curie point above room temperature.[2,3] Until now, however, a clear connection between magnetic properties and electronic structure has not been established and questions on the ferromagnetism being associated with clustering or incipient formation of secondary phases still persist. Thus, the extraordinary ability of single-phase films of Co-doped CeO_2, optically transparent in the visible spectral region, to exhibit ferromagnetism above room temperature (RT) with a quite large magnetic moment, as recently reported by Tiwari *et al.*,[4] represents a major step toward a suitable spin filter for semiconductor spintronics. A possible origin for the remarkable ferromagnetism of Co-doped CeO_2 resides in the hypothesis that Co^{2+} ions should be incorporated into Ce^{4+} sites with the concomitant formation of oxygen vacancies. However, Co^{2+} ions have a much smaller size compared to Ce^{4+} ions and a large distortion of the surrounding lattice will occur, facilitating defect migration of the matrix (i.e., CeO_2).

In this Rapid Communication, we describe the structural, electronic, and magnetic properties of nanocrystalline Co-doped CeO_2 films prepared by electrodeposition on Si(001) substrates. Apart from the fundamental physics behind the ferromagnetism of this system, our aim is to demonstrate that, among the various processing techniques used to prepare cerium oxide films onto a variety of important substrates,[4] electrodeposition is an attractive method for low-cost synthesis at low processing temperatures.

The electrochemical experiments were performed at RT using a stationary three-electrode cell with a galvanostat or potentiostat (EG&G model 273A). The working electrodes were rectangular slices (4×5 mm^2) of commercial single-side polished *p*-type Si(001) with a resistivity of 10 Ω cm at room temperature, which have been H terminated by removal of the native oxide via chemical HF etching prior to the electrodeposition experiments. A standard Ag/AgCl electrode was used as the reference while a platinum disk was used as the counterelectrode. Co-doped ceria films were cathodically deposited from twice-distilled aqueous solutions containing different amounts of $CeCl_3\cdot7H_2O$ (800 μmol/l Ce) and $CoSO_4\cdot7H_2O$ (from 800 to 50 μmol/l Co). Gallium-aluminum alloying was used on the rear of the Si slices to form a good Ohmic contact. A systematic study of the experimental parameters was done to find optimal conditions to obtain homogeneous cerium oxide films from solutions with $p\mathrm{H}<7$, where both free Ce^{3+} and Co^{2+} ions are stabilized.[5,6] A variety of current densities, reagent concentrations, and temperatures were studied using potentiostatic, galvanostatic, and potentiodynamic modes. Ce^{3+} ions in aqueous solution form a hydroxide $Ce(OH)_2{}^{2+}$ turning the solution a light orange. Ce^{4+} hydroxide ions in the solution close to the working electrode surface react with OH^- ions and CeO_2 is precipitated and deposited.[5,6] All samples here described were grown at *p*H values between 3.5 and 4.0 by addition of an appropriate amount of H_2O_2 and a cathodic potential of -1.0 V for 10 min. After the deposition, the substrates were thoroughly rinsed with distilled water and dried in air. The films are adherent, uniform, and translucent. It should be noted that a fresh solution must be used every time for electrodeposition because the solution very easily becomes a mixture of cerium hydroxide and cerium oxide. The chemical composition of deposits having 0.5 to 37.5 at. % Co was analyzed by energy-dispersive x-ray spectroscopy (EDS) using an electronic microscope JEOL JSM 6360-LV and x-ray photoelectron spectroscopy (XPS) analyses using a VG ESCA3000 spectrometer equipped with unmonochromatized Mg and Al x-ray sources and a hemispherical energy analyzer with an overall resolution of 0.8 eV at a 45° emission angle. The uncertainty in the compositional measurements are $\sim$1 at. % for XPS and $\sim$0.2 at. % for EDS.

Transmission electron microscopy (TEM) analyses and the selected area electron diffraction (SAED) of the deposits were performed using a JEOL JEM 1200EX-II operating at 120 kV. Figure 1 shows a bright-field TEM image of a de-

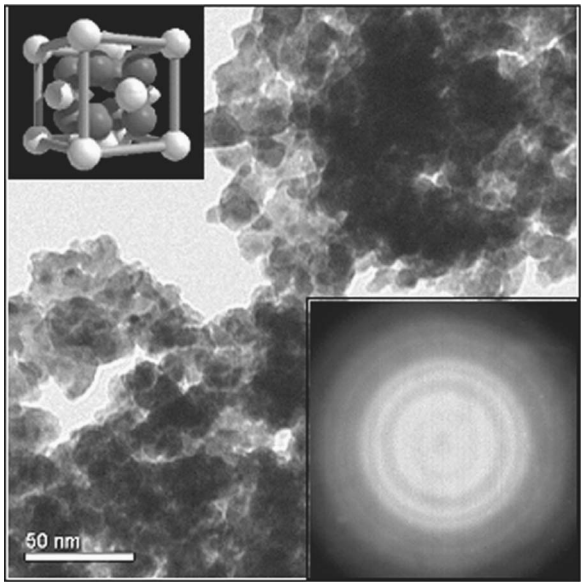

FIG. 1. Bright-field TEM image of CeO_2 film with 13.2 at. % Co. The upper left inset shows a unit cell of CeO_2 with light-gray and dark-gray spheres representing Ce and O atoms, respectively. The lower right inset shows the corresponding SAED pattern, which reveals the most intense diffraction rings of nanocrystalline CeO_2.

posit removed from the substrate by lift-off and carefully deposited onto a microscopy grid. A nanocrystalline structure is revealed, whereas the SAED pattern of the corresponding area indicates the presence of CeO_2. The mean size of CeO_2 nanocrystallites is ~14 nm (from 5.7 to 24.3 nm). Wide and diffuse diffraction rings indicate that the deposits include a significant amount of an amorphous phase; however, the spread of interplanar spacings determined from the width of the ring diameters is clearly associated with the strongest Bragg-reflection peaks of CeO_2, i.e., the (111), (002), (022), (113), and (222) planes, with cubic fluorite-type structure (ICDD International Centre for Diffraction Data database no. 28785), without evidence of Ce_2O_3, $Ce(OH)_4$, or CoO compounds or even metallic cobalt for the different samples.

In the XPS analyses the binding energy scale was calibrated to that of the Si $2p_{3/2}$ photopeak of bulk Si (99.3 eV) to correct energy shifts due to charging effects. Figures 2(a) and 2(b) show the photoelectron spectra of Ce 3*d* and Co 2*p* regions for three samples with different Co content, respectively. The spectra were collected right after turning on the x-ray source to avoid any x-ray-induced artifact, associated with oxygen-vacancy generation, as reported in the literature.[7–9] The spectral features attributed to pure, fully oxidized, and crystalline CeO_2, according to Engelhard *et al.*,[10] are indicated in the Ce 3*d* region. For low Co content a characteristic electronic structure of reduced nanocrystalline CeO_2 with distinctive features of Ce^{4+}, namely, the *U*‴ peak and the *V* and *U* splitting distance of 18.3 eV is observed.[5,10] These spectral features attributed to Ce^{4+} remain for increasing Co content. However, there are systematic increases of *U*′ and *V*′ spectral features, indicating the presence of Ce^{3+}. This observation corroborates the high concentration of oxygen vacancies in nanocrystalline ceria.[11] The increase of Co

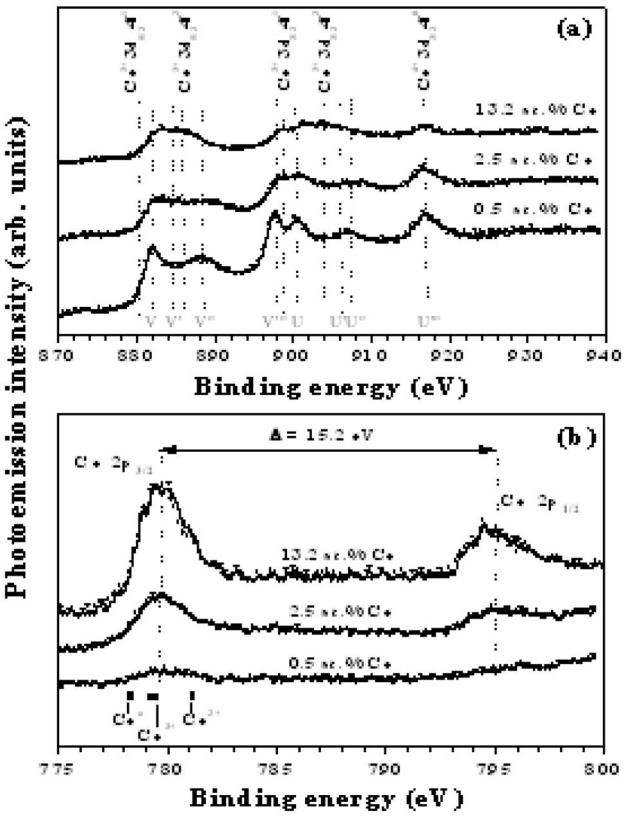

FIG. 2. (a) Ce 3*d* XPS spectra and (b) Co 2*p* XPS spectra for three Co-doped CeO_2 films. The letters *U* and *V* refer to the $3d_{5/2}$ and $3d_{3/2}$ spin-orbit components as conventionally adopted for pure CeO_2 in the literature. Distinct spectral features for Ce^{3+} and Ce^{4+} components are also shown. The Co $2p_{3/2}$ binding energy position for metallic Co^0, Co^{2+}, and Co^{3+} components are also indicated as solid bars.

content significantly favors the reduction of Ce^{4+} to Ce^{3+}. The spectra of the Co 2*p* region reveal a predominance of the Co^{3+} component whatever the Co content in the films. However, there are some weaker features corresponding to Co^0 (clearly, for 31.4 at. % Co) and Co^{2+} components. A similar spin-orbit splitting of ~15 eV is found for the three spectral components. There is no evidence of the shake-up satellite peak at about 6 eV from the Co $2p_{3/2}$ component at 780.2 eV, which is a signature of CoO (Ref. 12) and of CoO_x/CeO_2 (x=0.010 to 0.075) nanocomposites with grafting of CoO_x to CeO_2.[13] Therefore, our electrochemical route leads to spectral features rather distinct from those reported for the sintering of mixed oxides,[7,13,14] where the most favorable position of Co^{3+} doping atoms in the CeO_2 matrix is at Ce^{3+} sites next to an oxygen vacancy.

Raman spectroscopy experiments were performed at RT in the backscattering configuration using a micro-Raman system. As the excitation source the 514.5 nm (2.41 eV) line of an Ar^+ laser was used, focused on a 10 μm spot, with spectral resolution 4 cm^{-1}. The power density was kept under 10^5 W/cm^2 to avoid heating effects of sample and substrate. Ceria shows six optical-phonon branches in its dispersion, with only three zone center frequencies.[15] Figure 3 shows Raman spectra of Co-doped CeO_2 films with different Co

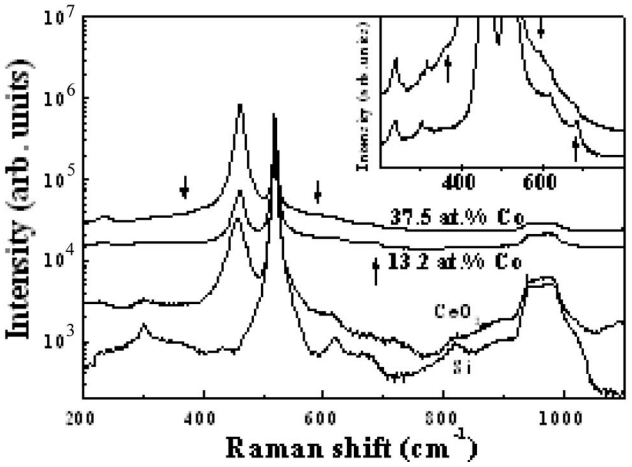

FIG. 3. Raman spectra of Co-doped CeO_2 samples with two different Co concentrations. The inset shows the Raman spectra with a more suitable intensity scale to observe both the LO Si and LO CeO_2 modes, at 520 and 462 cm^{-1}, respectively. The arrows in the Co-doped samples indicate features that find no equivalents in the pure CeO_2 or Si Raman spectra.

concentration, as well as of a pure CeO_2 sample. The Si substrate spectrum was added for comparison purposes. For the sake of clarity the spectra were vertically displaced. In the Si substrate Raman spectrum one can observe a number of peaks besides the main longitudinal optical (LO) mode at 520 cm^{-1}. All these peaks are due to second-order Raman scattering.[16] CeO_2 has only one allowed Raman-active mode with F_{2g} symmetry, which along with the Si LO phonon mode at 520 cm^{-1} from the substrate, is the most pronounced feature for the CeO_2 samples in the figure, and it is localized at about 462 cm^{-1}. This mode represents a symmetric "breathing" mode of the O atoms around each Ce and due to its symmetry it is nearly independent of the cation mass. In a previously reported study,[17] a shift of only 1 cm^{-1} after substituting the cation by one with 65% larger mass compared to Ce was observed. The case of Co entering the CeO_2 lattice in a substitutional Ce site would not be possible to follow from the Raman spectra by observing the main 462 cm^{-1} peak since almost no displacement of this peak is observed for the samples shown here, regardless of the Co concentration. The full width at half maximum of the 462 cm^{-1} peak is about 18 cm^{-1} for both spectra and their small asymmetry, of about 1–2 cm^{-1} for the Co-doped samples, can be attributed to the loss of translational symmetry of the crystal caused by either Co or defects in the CeO_2 lattice. We observe also an asymmetry in the Raman line of the pure CeO_2 sample. The arrows in the spectra indicate features that find no equivalent in pure CeO_2 or Si Raman spectra. The inset shows the Raman spectra for Co-doped samples with a more suitable intensity scale in order to observe these modes. Both the LO Si as well as the CeO_2 modes, at 520 and 462 cm^{-1}, respectively, extrapolate to the view window. The peaks at about 302 and 610 cm^{-1} are due to the Si substrate and they are attributed to 2TA(X) and a combination of acoustic and optic phonons in the Σ direction respectively, as second-order processes.[16] Besides these two peaks it is possible to observe two other features at about 237 and 684 cm^{-1}. We attribute

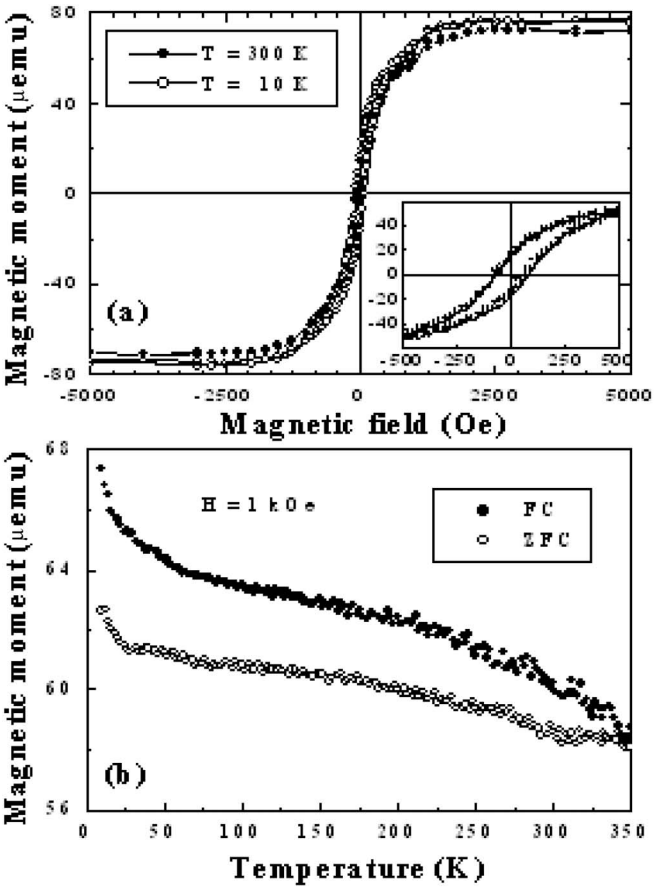

FIG. 4. (a) Hysteresis loops measured for CeO_2 film with 13.2 at. % Co. The inset shows the inner part of the loops. (b) FC and ZFC curves indicating a ferromagnetic state with critical temperature above 350 K.

these to 2TA(L) and 2LO$_R$(X) second-order processes of CeO_2.[15] For the sample with higher Co concentration we observe a mode at about 380 cm^{-1} and a second one at about 580 cm^{-1}. The former can be attributed to a second-order process of 2TA(X). The appearance of the many second-order Raman scattering processes in these spectra is a direct consequence of the inclusion of Co or other defects into the lattice and consequently a loss of translational symmetry. This leads to the invalidation of the $k=0$ wave vector selection rule for Raman scattering and phonons of all parts of the Brillouin zone. The mode at about 580 cm^{-1} can be attributed to defects introduced into the lattice whenever a Ce^{4+} is substituted for a Ce^{3+}.[16–18]

All magnetic measurements were performed using a superconducting quantum interference device (SQUID) magnetometer (Quantum Design MPMS-5S) with applied magnetic field parallel to the sample surface. Zero-field-cooling (ZFC) and field-cooling (FC) magnetic moment curves were obtained during warming up at a rate of 2 K/min. Figures 4(a) and 4(b) show the hysteresis loops and temperature dependence of the field-cooling and zero-field-cooling magnetic moment for a film with 13.2 at. % Co, respectively. The absence of a maximum in the ZFC sample (blocking temperature) is an indication that superparamagnetic Co nanoparticles are not present in the sample.The observed magnetic

irreversibility (bifurcation between the FC and ZFC curves) comes from the low cooling field compared to the saturation one and the incomplete demagnetization of the sample at 350 K. Deposits with different amounts of cobalt confirm a characteristic ferromagnetic behavior with RT remanence and saturation field of about 5 kOe. Even samples containing ~2.7 at. % Co exhibit a robust ferromagnetic behavior at RT. Magnetic moment estimation gives less than $1\mu_B$ per Co atom for samples having more than 13.2 at. % Co, probably due to Co oxide formation. Samples with lower Co content, particularly ~5 at. % Co, exhibit atomic magnetic moment as high as $(4.9\pm0.9)\mu_B$ per Co atom at 10 K. In contrast with ferromagnetism reported for several nondoped oxides[19] including CeO_2 nanoparticles,[20] our pure CeO_2 films are paramagnetic at RT, probably because they are almost fully oxidized. Therefore, the issue of whether high-spin point-defect centers associated with Ce vacancies could promote the occurrence of ferromagnetism at RT as described by Das Pemmaraju and Sanvito[21] appears to us as suitable as the framework of a percolated network of bound magnetic polarons proposed by Kaminski and Das Sarma.[22] In the latter, the localized charge carriers are equally either holes or electrons for the exchange interaction of localized carriers with magnetic Co impurities. It is instructive to point out that our relative magnetization as a function of the temperature is in good qualitative agreement with the magnetization behavior predicted by Ref. 22.

In conclusion, the presence of cation defect centers and oxygen vacancies corroborates the Raman and XPS analyses shown above. The Curie temperature above RT at doping levels below the physical percolation threshold must somehow be associated with underlying exchange mechanisms instead of Co clustering or incipient formation of secondary phases. Our analysis suggests that the ferromagnetism is intrinsically related to a mixture of core-hole and valence-hole states with the mixed-valent (Ce^{4+}, $4f^0$) spin singlet and (Ce^{3+}, $4f^1$–O $2p$ hole) electronic ground states as revealed by XPS analyses. Thus, the occurrence of ferromagnetism in Co-doped CeO_2 with mixed-valent states results from two concomitant intrinsic-defect mechanisms of exchange interaction, where Co^{3+} replacing Ce^{3+} and stabilized around oxygen vacancies originates high-spin localized states with a robust ferromagnetic ground state for the whole system.[21,22] The connection between magnetic properties and electronic structure, as well as the material compatibility with silicon, render Co-doped CeO_2 films on Si very attractive for multifunctional spintronic applications.

Financial support by the CNPq, PRONEX-Fundação Araucária, and FAPESP (Grants No. 04/08524-0 and 03/09933-8) is acknowledged. The authors acknowledge the technical support of Centro de Microscopia Eletrônica da UFPR in the TEM measurements. Raman measurements were performed at Laboratório Institucional de Espectroscopia Raman da UFPR.

*Electronic address: mosca@fisica.ufpr.br

[1] S. A. Wolf, D. D. Awschalom, R. A. Buhrman, J. M. Daughton, S. von Molnár, M. L. Roukes, A. Y. Chtchelkanova, and D. M. Treger, Science **294**, 1488 (2001).

[2] J. M. Coey, C. M. Venkatesan, and C. B. Fitzgerald, Nat. Mater. **4**, 173 (2005).

[3] J. Philip, A. Punnoose, B. I. Kim, K. M. Ready, S. Layne, J. O. Holmes, B. Satpati, P. R. Leclair, T. S. Santos, and J. S. Moodera, Nat. Mater. **5**, 298 (2006).

[4] A. Tiwari, V. M. Bhosle, S. Ramachandram, N. Sudhakar, J. Narayan, S. Budak, and A. Gupta, Appl. Phys. Lett. **88**, 142511 (2006).

[5] A. Q. Wang and T. D. Golden, J. Electrochem. Soc. **150**, C616 (2003); **150**, C621 (2003).

[6] I. Zhitomirski and A. Petric, Mater. Lett. **40**, 263 (1999), F. B. Li and G. E. Thompson, J. Electrochem. Soc. **146**, 1809 (1999); Y. Zhou, R. J. Philips, and J. A. Switzer, J. Am. Ceram. Soc. **78**, 981 (1995).

[7] L. F. Liotta, G. Di Carlo, G. Pantaleo, A. M. Venezia, and G. Deganello, Appl. Catal., B **66**, 217 (2006).

[8] A. E. Hughes, J. D. Gorman, P. J. K. Patterson, and R. Carter, Surf. Interface Anal. **24**, 634 (1996).

[9] A. Galtayries, R. Sporken, J. Riga, G. Blanchard, and R. Caudano, J. Electron Spectrosc. Relat. Phenom. **87**, 31 (1997).

[10] M. Engelhard, S. Azad, C. H. F. Peden, and S. Thevuthasan, Surf. Sci. Spectra **11**, 73 (2004).

[11] L. Qiu, F. Liu, L. Zhao, Y. Ma, and J. Yao, Appl. Surf. Sci. **252**, 4931 (2006).

[12] M. Ghosh, E. V. Sampathkumaran, and C. N. R. Rao, Chem. Mater. **17**, 2348 (2005).

[13] M. M. Natile and A. Glisenti, Chem. Mater. **17**, 3403 (2005).

[14] T. Zhang, P. Hing, H. Huang, and J. Kilner, J. Eur. Ceram. Soc. **22**, 27 (2002).

[15] W. H. Weber, K. C. Hass, and J. R. McBride, Phys. Rev. B **48**, 178 (1993).

[16] P. A. Temple and C. E. Hathaway, Phys. Rev. B **7**, 3685 (1973).

[17] J. R. McBride, K. C. Hass, B. D. Poindexter, and W. H. Weber, J. Appl. Phys. **76**, 2435 (1994).

[18] A. Nakajima, A. Yoshihara, and M. Ishigame, Phys. Rev. B **50**, 13297 (1994).

[19] N. H. Hong, J. Sakai, N. Poirot, and V. Brize, Phys. Rev. B **73**, 132404 (2006).

[20] A. Sundaresan, R. Bhargavi, N. Rangarajan, U. Siddesh, and C. N. R. Rao, Phys. Rev. B **74**, 161306(R) (2006).

[21] C. Das Pemmaraju and S. Sanvito, Phys. Rev. Lett. **94**, 217205 (2005).

[22] A. Kaminski and S. Das Sarma, Phys. Rev. Lett. **88**, 247202 (2002).